Chemically functionalised suspended-core fibre for ammonia gas detection

LiangLiang Liu, Zijuan Tang, Chenyang He, Serhiy Korposh, Shuqin Lou, and Stephen P. Morgan*

***Abstract*— An optical fibre ammonia gas sensor utilising a functionalised four-leaf-clover-shaped suspended-core fibre (SCF) is demonstrated. The fibre is functionalised by depositing a thin layer of an ammonia sensitive dye (tetraphenylporphyrin tetrasulfonic acid hydrate) (TPPS) on the wall of the inner cavities of the SCF through capillary action. An in-line fibre sensing structure is designed for light transmission through the SCF and also allows gas exchange with the atmosphere through two porous polyethylene housings. The sensing structure exhibits a temperature-dependent transmission due to the thermal expansion of the housings. A ratiometric method is applied for signal processing which is demonstrated to reduce significantly the effect of temperature change in the tested range (20-30 ˚C). The sensor is tested in ammonia concentration ranges from 0-10 ppm and demonstrates capability of detecting ammonia at ppb levels. The minimum tested concentration is 150 ppb in the experiment with a calculated limit of detection of 20 ppb. The sensor response time ($T_{10-90\%}$) is 160 s and it is demonstrated to be reusable after treatment with hydrogen chloride vapour. Numerical simulation of evanescent absorption features of such an SCF indicates that approximately 0.02% of the optical power exists in the air holes for the fundamental propagation mode. Distinctive absorption bands observed in the transmission spectrum of the fabricated sensor can also be observed in the simulated model after adding the TPPS absorption layer in the holes.**

Keywords: microstructured fibre sensor, chemical sensor, gas sensor, suspended-core fibre, ammonia sensor.

I. Introduction

Gas sensing with optical fibre sensors is becoming a popular approach in many fields of application such as environmental monitoring [1], industry [2] and healthcare [3-5] due to their comparable sensing performance to traditional electrochemical and semiconductor gas sensors, and distinctive advantages such as compact size, remote sensing, multiplexing and immunity to electromagnetic interference. They are particularly favoured for sensing in hazardous environments such as coal mines where electrical sparks are dangerous in an explosive atmosphere [6], and in healthcare where minimally invasive measurement is necessary [7].

A holey fibre or microstructured optical fibre is characterised as an array of air holes distributed in the cladding region along the entire length of an optical fibre. It has a strong wavelength dependence on the cladding refractive index that renders unique properties including high nonlinearity [8], endlessly single-mode operation [9] and high birefringence [10] depending on the specific arrangement of the holes. For these reasons, holey fibres are considered good candidates for applications in optical communications and nonlinear optics. They are also extremely useful in sensing due to the extended evanescent field in the air holes which removes the need for fibre reshaping typically required by other evanescent sensors such as cladding removal [11] or tapering [12]. This shaping exposes the evanescent field for sensing but makes the sensing region fragile. Proposals have been made for sensing gases and liquids by using holey fibres where the analytes travel through the holes and interact with the optical field or sensing materials [13-20]. Due to the high interaction length and increased evanescent field, sensors based on holey fibres have the potential to provide high sensitivity [21]. Another advantage is that such interactions are not disturbed by external contaminations (e.g. water, dust, oil), damage or ambient light as they occur within the holes of the fibre where the electric field is confined. This is particularly true for an optical fibre sensor with functional layers, and important for sensor applications required in the ground, or in the sewer where contamination is highly likely. In healthcare applications where sensors are needed to be implanted or in contact with human tissues [3], microstructured fibres are robust and create a means of protection for any non-biocompatible sensing materials.

Ammonia detection is significant in safety monitoring of the workplace due to its toxicity to human health. For example, there is a high risk of ammonia exposure in the livestock and fertiliser industries [22]. The long-term exposure limit of ammonia is 25 ppm according to the US Agency for Toxic Substances and Disease Registry [23]. The strategies to develop an optical ammonia gas sensor lay in two categories that are gas absorption spectroscopy and sensitive coating assisted detection. The former is based on the natural absorption of ammonia to light with a frequency matching the resonance frequency of the gas molecules. This typically comes with a configuration of a gas cell in an optical path and measures attenuation in the UV [24], near-infrared [25], or mid-infrared wavelength regions [26]. The light beam is collimated with a lens for propagation within the cell. Microstructured optical fibres can be applied for gas absorption measurement in which the gas cell is replaced with a section of the holey fibre to form an in-line sensing system in order to reduce the size of sensing system [21]. For example, a hollow optical waveguide is

This work was supported by the Medical Research Council, U.K. under Grant MR/R025266/1. The manufacture of the suspended-core fibre is supported by the National Science Foundation of China (Grant No. 61775014).

L. Liu, C.He, S.Korposh and S.P.Morgan are with the Optics and Photonics research group, University of Nottingham, UK (e-mail: liangliang.liu1@nottingham.ac.uk, chenyang.he2@nottingham.ac.uk, s.korposh@nottingham.ac.uk, steve.morgan@nottingham.ac.uk).

Z. Tang and S. Lou are with School of Electronic and Information Engineering, Beijing Jiaotong University, China (email: 17111024@bjtu.edu.cn, shqlou@bjtu.edu.cn)

applied for ammonia gas absorption detection as the 'gas cell' which removes the need for a collimation lens but has a long optical path (3 m) [27].

An alternative approach for optical fibre ammonia gas sensing is functionalisation of an optical fibre with a thin sensitive layer whose optical properties (refractive index, absorption or fluorescence) change in the presence of ammonia [28-31]. This allows gas sensing in the visible wavelength range that can be easily implemented in conventional silica optical fibre and reduces costs. Sensitivity can be enhanced by combining with plasmonic techniques [32]. Taking advantage of the sensitive response of the chemical layer, the sensor requires only a short length of optical fibre as the sensing region (typically < 10 cm). For example, an optical fibre Fabry-Pérot sensor which has a section of microstructured optical fibre (~700 µm) as the sensing cavity is reported for detection of ammonia. The holes of the fibre are sputter coated with an SnO2/ITO nanofilm which changes its refractive index in response of ammonia leading to a shift of interference wavelength [28]. A fluorescent ammonia sensor based on microstructured optical fibre is reported by modifying the fibre with fluorescent dye [33]. However, it is an optically open space set-up in which excitation of the dye is performed with side-illumination perpendicular to the fibre and requires a lens for light collection. This configuration is complex, relatively bulky and requires operation in dark conditions. The suspended core fibre (SCF) is the optimal design amongst microstructured optical fibres as it combines strong light-matter interactions within the intrinsic holes with a simple design with large air holes that are easy to fill with gases or liquids [34].

In this work, a new all-fibre ammonia sensor based on a microstructured optical fibre is reported by introducing a colourimetric measurement of ammonia into an in-line structured optical fibre sensing system. A thin layer of colourimetric dye, tetraphenylporphyrin tetrasulfonic acid hydrate (TPPS), is deposited in the inner wall of the holes of a four-leaf-clover-shaped SCF by the means of capillary action. Compared to the previously described fluorescent sensor [33], the advantage of using the absorbing dye is that it reacts with ammonia directly whereas the fluorescent dye requires moisture participation which is not always available and controllable in practical scenarios. The all-fibre sensing design provides compact, portable and robust gas detection. It demonstrates high sensitivity to ammonia with a minimum detected concentration of 0.15 ppm in the experiment and a theoretical limit of detection of 0.02 ppm. The optical transmission of the SCF for evanescent sensing in conjunction with a thin absorption layer within the holes is studied with commercial software COMSOL Multiphysics. The ease of manufacture and simple configuration allows the approach to be adapted for different gas sensing purposes.

II. EXPERIMENTAL DESIGN AND PROCEDURE

A. *Ammonia-dye interaction*

The spectroscopic property of the TPPS molecules varies depending on the molecular protonation status as well as the aggregate format [35]. TPPS molecules form J-aggregate under acidic condition where the diprotonated monomeric molecules are arranged in one dimension with transition moments in parallel (side-by-side arrangement) due to the interplay of electrostatic and hydrogen-bonding interactions [36] (illustrated in Fig. 1). Ammonia tends to deprotonate the nitrogen atoms in the porphyrin core resulting in free base monomer with no charges. This disrupts interplay interaction such that a change of aggregate. And as a result, the spectroscopic property changes accordingly. Treatment with HCl retrieves the charge and restore the J-aggregate leading to a recovery of the spectrum.

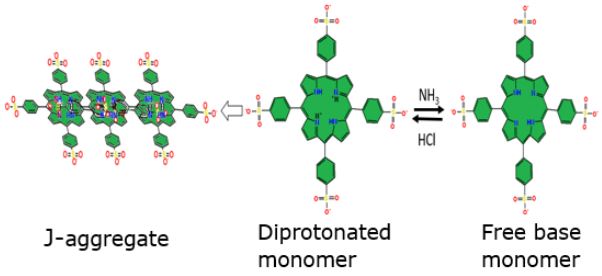

Fig. 1 Molecular change of TPPS during ammonia interaction. J-aggregate is formed under acidic condition.

B. *Design of the SCF ammonia sensor*

A ~10 cm length of silica four-leaf-clover-shaped suspended core fibre (Yangtze Optical Electronics) is firstly cleaved on both ends at 90 degrees with a mechanical cleaver. A few millimetres of one end of the cleaved fibre is then vertically immersed into a prepared TPPS solution (1 mM in water, Tokyo Chemical Industry) for few seconds until the entire fibre turns a jade green colour due to uptake of TPPS solution into the holes via capillary action (illustrated in Fig. 2). The liquid is held within the holes due to the surface tension after removal from the liquid. The liquid-filled fibre is subsequently placed into an oven in a standing position for 2 days at 70 °C to evaporate water solvent so that the TPPS film is then deposited on the wall of each hole within the fibre.

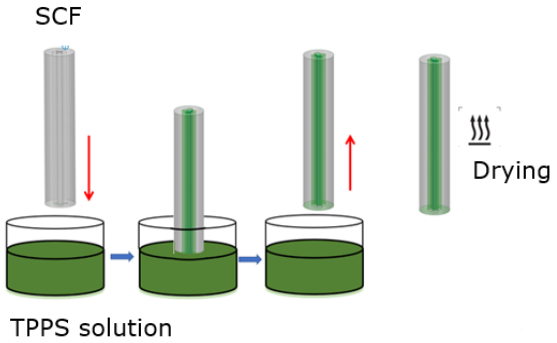

Fig. 2 The inner functionalisation process of the SCF. Uptake of the dye is through capillary action before placing in an oven (fibre length ~10 cm).

Once the drying process is completed, the fibre is cleaved again from both ends to ensure that no film remains at the end-facets. The two cleaved ends are inserted into two fibre optic ceramic

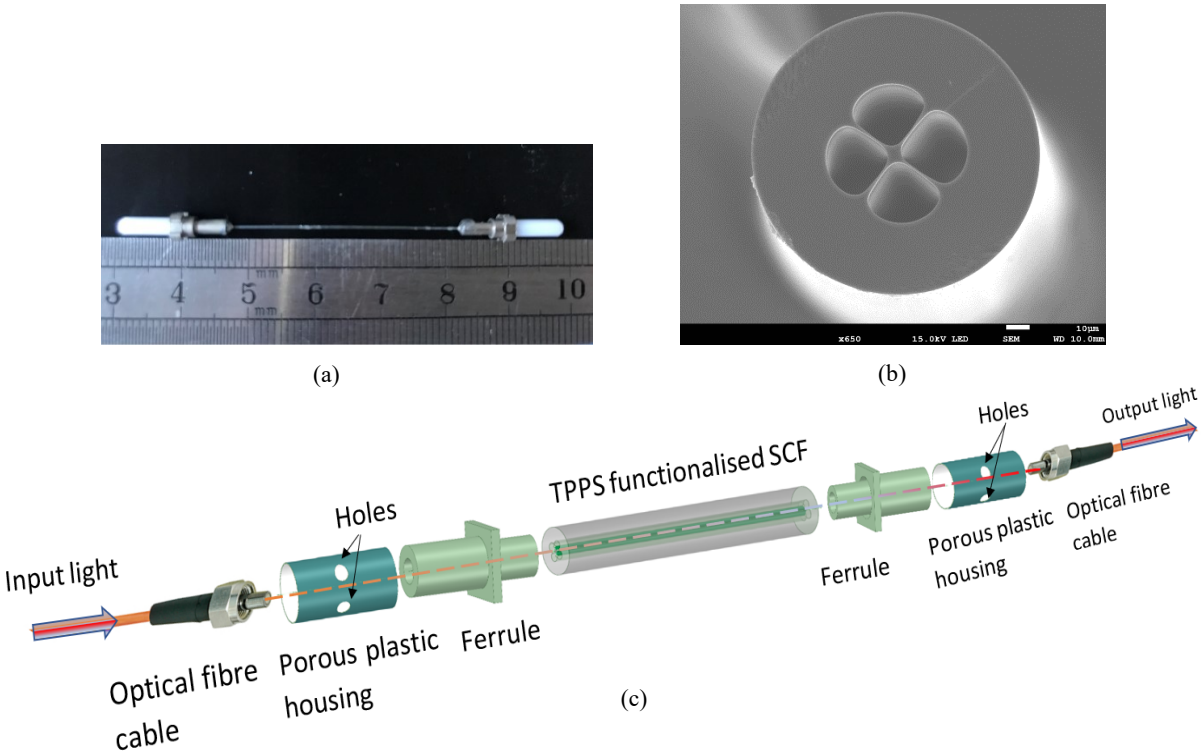

Fig. 3 (a) Functionalised SCF with two ends packaged with fibre optic ferrules. (b) cross-section of the SCF under SEM (scale bar=10 μm). (c) The schematic break-up of the optical connection for the functionalised SCF ammonia sensor.

ferrules with the end-facet level with the end of the ferrule, and fixed with epoxy resin from the back. An image of the sensing fibre is displayed in Fig.3a and the total length of the coating fibre available for sensing is 7 cm (after the second cleaving). The image in Fig.3b shows the cross-section of SCF observed under a scanning electron microscope (JEOL, JSM-7100F). The average radius of core and sector-shaped hollow leaves are ~3.4 μm and 26 μm, respectively.

The breakdown of the SCF ammonia sensor is shown in Fig.3c where the functionalised SCF is connected in the middle of an optical pathway via two plastic housings (made of Polyethylene) that are machined with 2 pairs of orthogonal holes (Ø 1 mm). A multimode optical fibre cable (Ø 62.5/125 μm, All4fibre) that transmits light from a halogen light source (HL-2000, Ocean Insight) connects to the functionalised SCF via the plastic housing with a gap between the two ferrules (~1 mm) right below the machined holes. Fixation is achieved with epoxy resin on both ends of the housing to avoid movement of the ferrules in the housing. The other end of the SCF is likewise connected to a CCD spectrometer (Flame, Ocean Insight) via a multimode optical fibre. There is an open-air pathway from the machined holes, through the gap in the connection point and into the air holes of the SCF. The light emerging from the SCF then similarly passes out of the machined holes of the second housing via an open-air pathway and into the spectrometer. Gas diffuses into the holes of SCF and interacts with the functional coating as the light passes through the solid core. The optical changes induced by the chemical interaction between the functional coating and target gas are captured and represented on the transmission spectrum from the spectrometer.

C. *Evanescent sensing with SCF*

The transmission intensity of the SCF sensing structure with the incorporation of the functional layer (TPPS film) coated inside of the holes is defined by the Beer-Lambert law:

$$I = I_0 \exp(-aL) \quad (1)$$

Where I_0 is the intensity in the absence of the dye, L is the length of the functionalised SCF and a is the evanescent-absorption coefficient of the dye. An optically absorbing material such as colorimetric dye has a complex refractive index of $N = n - ik$, where the imaginary part is the extinction coefficient (k) attributes selective absorption of the dye to certain wavelengths of light. The absorption coefficient (a') is related to the material extinction coefficient through [37]:

$$a' = 4\pi k/\lambda \quad (2)$$

In this work, finite element analysis is conducted with COMSOL Multiphysics which performs mode analysis in a defined geometry and the loss of a particular waveguide mode is reflected in the imaginary part of the effective mode refractive index. Therefore, the normalised intensity or transmission value (T), in this case, can be rewritten as [38]:

$$T = \frac{I}{I_0} = \exp(-\frac{4\pi}{\lambda} imag(n_{eff})L) \quad (3)$$

Where n_{eff} is the effective mode index and L is the interaction length. The extinction coefficient of TPPS at different wavelengths is obtained through an absorption spectroscopic measurement of a TPPS thin film on a glass substrate with known film thickness by using Eq.(2). The real part of the refractive index of TPPS is negligible compared to the

transmission value and is set as 1.3 in the simulation. The TPPS film thickness deposited on the wall of the holes is estimated as ~3 nm. This calculation is based on knowing the total mass of TPPS infused in the holes, the overall surface area and density of the TPPS and assumes that the film is evenly deposited over the inner surface of the holes.

D. Experimental Procedure

To investigate the ammonia measurement performance, the SCF sensor is placed in a sealed acrylic chamber (dimensions: 21 cm × 21 cm × 10 cm) along with the commercial reference sensor (4-NH3-100, Honeywell). Different concentrations of ammonia gas (up to 10 ppm) are generated by injection of different volumes of 1% wt ammonia aqueous solution (2, 4, 8, 15 and 30 µL) into the chamber at ambient temperature. For the reversibility test, the sensor is initially exposed to a high concentration of ammonia gas (53 ppm, generated with 2 µL of 28% wt ammonia aqueous solution in the chamber) to obtain the ammonia response time, and then hydrogen chloride (HCl) vapour (generated with 10 µL of 37% HCl solution inside the chamber) to observe the recovery of the sensor. The response time ($T_{10\text{-}90\%}$) and recovery time ($T_{90\text{-}10\%}$) are calculated as the time between 10% to 90% and 90% to 10% of signal change, respectively. To test the repeatability of the sensor, the sensor is repeatedly exposed to the same concentration of ammonia with HCl vapour for recovery. All spectra are processed with a moving average filter (window size: 20 points) so that the high-frequency component of the interference pattern due to the air gap between optical connections is removed.

The temperature response of the sensor is tested with a temperature-controlled chamber (CVMS Climatic) with the temperature set in the range of 20-30 ºC which covers typical indoor ambient temperature fluctuation. Sensor spectra are taken when the signal stabilises at a specific temperature for at least 5 mins. A second sensor is fabricated with the same optical connection but with no dyes applied in the SCF, and tested following the same temperature test procedure.

III. RESULTS

A. Simulation of SCF ammonia sensor

Figs. 4a and b show the electric field distribution of the fundamental transmission mode in the SCF model described in Section. II.B which uses geometrical information measured from the SEM image (Fig. 3b) for the core and air holes with a perfectly matching layer as an outer layer. It can be seen that the electric field extends from the core into the air holes. The optical power that leaks into the four air holes, as a proportion of the whole cross-sectional area for different wavelengths is plotted in Fig. 4c which is approximately 0.02% at a wavelength of 703 nm. We have calculated 50 propagation modes in the simulation model and only the fundamental mode can steadily propagate through the SCF fibre with the transmission of 100% whereas other higher modes have high loss and almost zero transmission for a given length (7 cm). Therefore, higher modes are ignored. Fig.4d shows the electric field in a drawn line across the air holes and the solid core (inset figure) for the operation wavelength of 703 nm with and without the TPPS coating. The electric field magnitude decreases after the TPPS coating is applied as a result of selective absorption of the dye. Fig. 4e shows the imaginary part of the effective mode index of different wavelengths for light propagation in the TPPS functionalised SCF sensor. In contrast to the non-functionalised SCF in which the imaginary part of mode index is zero, the TPPS functionalised SCF shows distinctive features in the imaginary part of the mode index with the peak positions matching the extinction features of the TPPS. Consequently, the transmission spectrum calculated from Eq.(3) exhibits two attenuation bands for the TPPS functionalised SCF sensor of different lengths whereas the bare SCF shows no loss in its transmission value (Fig. 4f).

B. Ammonia sensing

The transmission spectrum of the SCF ammonia sensor has distinctive attenuation bands at wavelengths λ= 703 nm and λ= 487 nm (black line in Fig. 5a), and these match well to the Q-band and Soret absorption band of TPPS in acidic solution (pH=1) (red dash line) indicating that the TPPS dye is successfully deposited inside the SCF. It also indicates that the TPPS molecules are presented in J-aggregate form after deposition on the fibre. In the experiment, the two distinctive attenuation bands corresponding to the Soret and Q-band of the dye are observed, and this is also seen in the simulation.

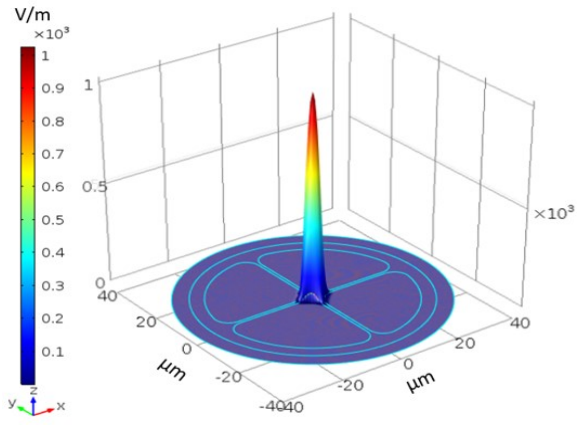

(a)

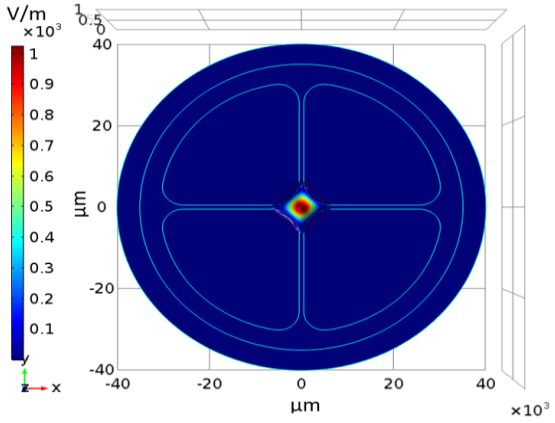

(b)

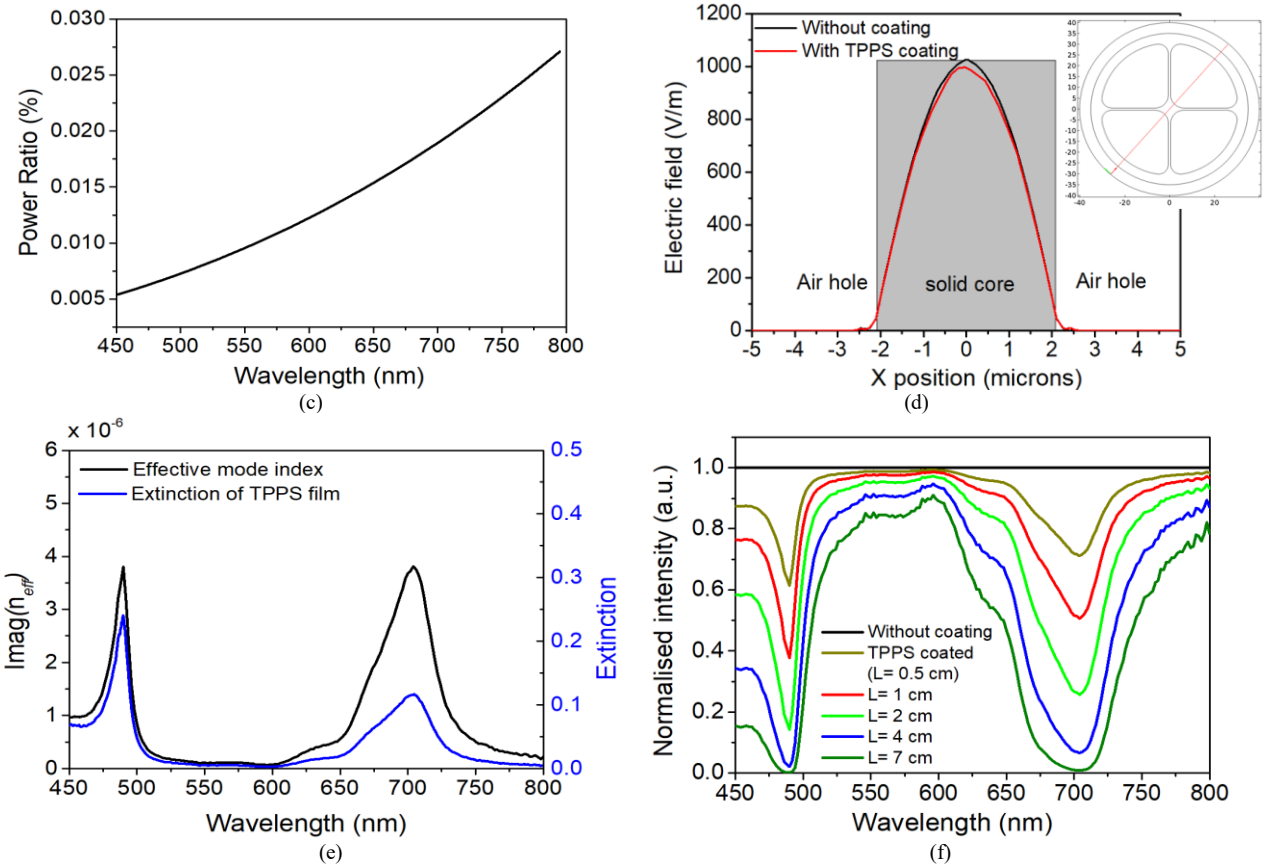

Fig. 4 (a)(b) Electric field distribution within the SCF (fundamental mode). (c) Optical power fraction inside the holes for different wavelengths. (d) The electric field along the drawn line (inset graph) across the region of air holes and solid core for the wavelength of 703 nm (fundamental mode). (e) The imaginary part of the mode refractive index at different wavelengths in comparison to the input material extinction. (f) The transmission spectra of the simulated SCF with different lengths.

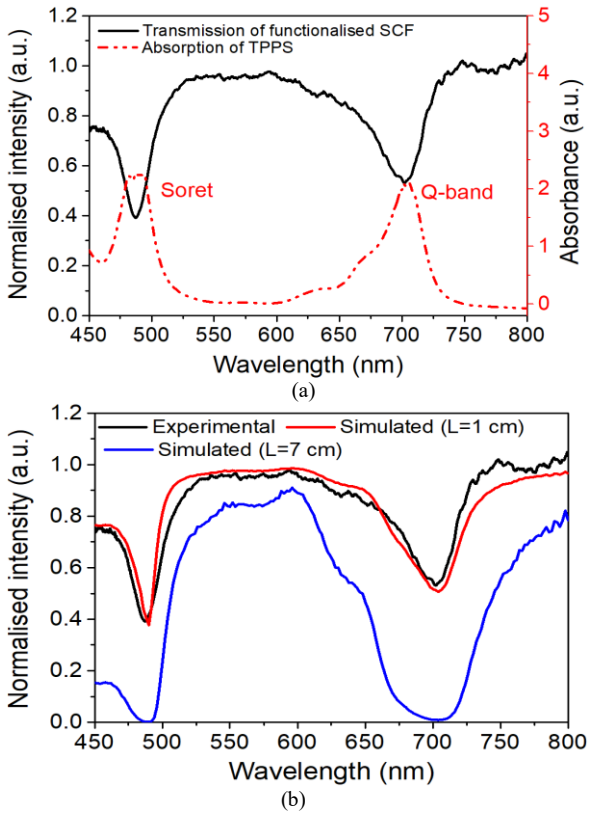

Fig.5 (a)Transmission spectrum of the SCF ammonia sensor (black). The intensity is normalised with the same optical connection with no dye applied. The red dash line is the absorption spectrum of TPPS water solution (0.03 mM, pH=1) measured with absorption spectroscopy. (b)Transmission spectrum obtained via experiment and simulation model.

As compared to the simulation results, the spectrum obtained in the experiment (fibre length = 7 cm) has lower attenuation at the two absorption bands for the same length of the fibre and they are closer to the simulated spectrum of a shorter length i.e. 1 cm (Fig. 5b). This may indicate that the dye coated inside of the fibre holes is less than its theoretical value with either non-uniform distribution or a thinner coating as the simulation model considers a uniform film-coated in the inner side of the fibre.

The normalised intensity at both wavelengths increases when the sensor is exposed to an ammonia atmosphere (53 ppm) with a magnitude change of 0.14 (14 %) and 0.11 (11%) for the wavelengths of 703 and 487 nm, respectively (Fig. 6a). This change is due to a deprotonation process in which ammonia molecules deplete protons from the porphyrin ring of TPPS molecules resulting in a spectral change as explained in Section. II.A. There is also a clear redshift ($\Delta\lambda$ = 6.2 nm) for the first attenuation band (Soret band) which corresponds to our previous observation in [29] due to the change of aggregate structure of TPPS molecules induced by the ammonia

interaction. Wavelengths that are outside the absorption region (e.g. λ= 800 nm) remain unchanged in the presence of ammonia. A ratio ($I_{703\ nm}$ /$I_{800\ nm}$) between the intensity of two wavelengths (λ= 703 nm and λ= 800 nm) is taken as the signal for tracking ammonia response. This helps to compensate for the potential drift of the light source which is a common problem for intensity-based measurements. Fig. 6b illustrates that the signal increases immediately upon exposure to ammonia (53 ppm) and gradually stabilises. The response time ($T_{10\text{-}90\ \%}$) is calculated as 160 s. The signal then decreases as HCl vapour is introduced and finally returns to its original position. The recovery time ($T_{90\text{-}10\%}$) is calculated as 225 s. The HCl vapour protonates the porphyrin ring of TPPS molecules that are temporally deprotonated by ammonia and turn the molecules back to their original status.

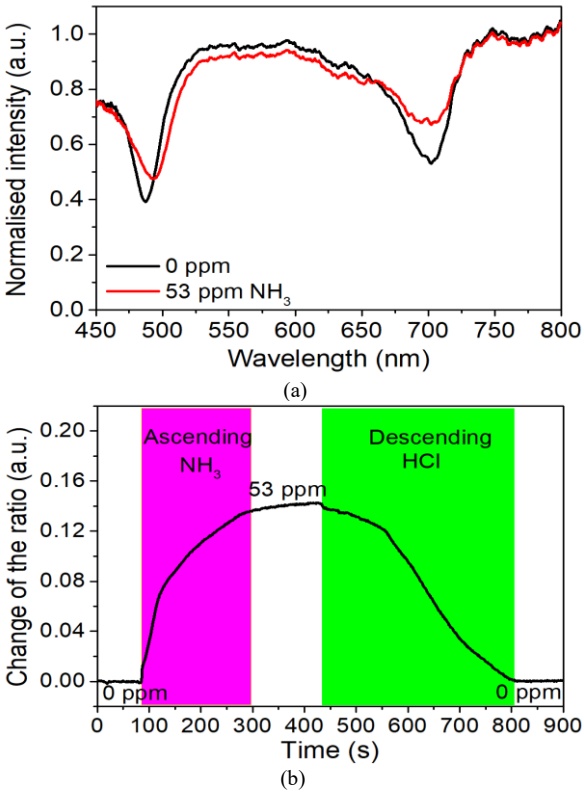

Fig.6 (a) Spectral response of the SCF sensor to ammonia. (b) The signal (intensity ratio) responds to ammonia and reverses upon exposure to HCl.

The spectral change to different concentrations of ammonia is shown in Fig. 7a. With increasing ammonia concentration there is an increase in the intensity of the central wavelength of the attenuation bands and a shift of the peak wavelength of the Soret band as observed similarly in Fig. 6a. In contrast, there is a small baseline drop with increase of concentration which is associated with the temperature change (as discussed in section. *C*). The change of the signal is plotted in Fig. 7b and the logarithmic curve fitting indicates that the sensor gradually reaches its saturation point beyond which the sensor is not able to distinguish the continuous increase of the concentration. The minimum tested concentration is 0.15 ppm at which the optical fibre sensor exhibits a measurable signal increase. The theoretical detection limit is estimated as 0.02 ppm at a signal-to-noise ratio of 3 when applying a linear fitting of the first three points whereas the noise is taken as the fluctuation of the intensity at blank. The inset graph of Fig. 7b shows the change of the signal to repeated exposure to the same concentration of ammonia with HCl treatment after each exposure. It demonstrates that the sensor can be reused after refreshing with HCl. Here we notice that the signal does not always return to the same position under HCl treatment and this variation may be associated with the incomplete transformation of TPPS molecules or residuals of ammonia in the fibre due to the 'sticky' property of ammonia gas [39].

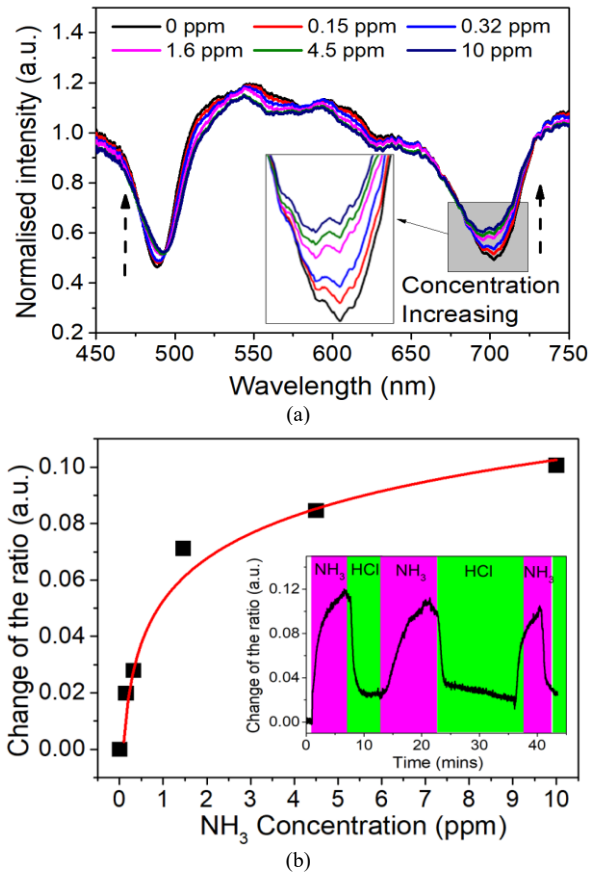

Fig.7 (a) Spectral response of the SCF sensor to different concentrations of ammonia. (b) The change of the ratio as a function of ammonia concentration (error bar is smaller than marker size). Inset graph shows the repeatable test of sensor to the same concentration of ammonia.

C. Temperature response

The developed SCF ammonia sensor shows dependence of its transmission intensity on temperature as shown in Fig. 8a. The overall intensity of the spectrum drops as temperature increases while the shape remains similar. The intensity of the reference wavelength (λ= 800 nm) at a specific temperature is plotted in Fig. 8b (spectra are normalised at 20 °C). A reversible change of intensity to temperature variations is observed and the repeatability of intensity at a specific temperature demonstrates that temperature measurement with the intensity of a single wavelength is feasible. The temperature-dependent transmission intensity is attributed to thermal expansion of the plastic housings that modulate the distance of two ferrules in the connection point resulting in different transmission efficiency. As temperature increases, the plastic housings

expand so that the gap between two ferrules increase and the amount of light transmitted from one ferrule to another is reduced. The intensity ratio ($I_{703\ nm}$ /$I_{800\ nm}$), however, remains relatively stable to temperature with variation <0.02 (corresponding to an ammonia concentration of 0.22 ppm). This indicates that temperature fluctuation within the detected range has minimal contribution to confound the ammonia detection. A separate temperature test (results not shown) with the same in-line fibre arrangement in Fig. 3c but with a bare SCF (without dye) has confirmed that the change of intensity due to temperature is from the optical fibre connection rather than the effect of the dye.

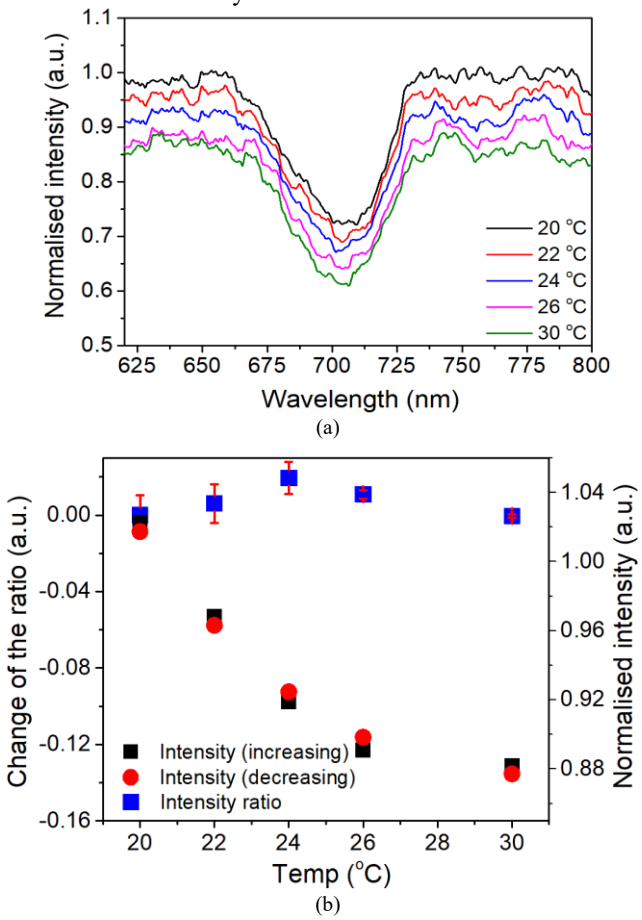

Fig. 8 (a) Spectral response of the SCF sensor to temperature. (b) The intensity change of a single wavelength (λ= 800 nm) as a function of temperature.

IV. Discussion

A new optical fibre ammonia sensor has been demonstrated by depositing a functional layer (TPPS) inside the holes of an SCF for spectroscopic analysis. Sensor optimisation such as the length of the SCF is not the focus of this work, however, it is a reasonable assumption that a longer SCF coated with TPPS will provide higher sensitivity due to the extended interaction length as seen from the transmission equation (Eq. (3)). The tradeoff is an increase in the response time due to the long travel distance of gas diffusion. There is also a limit to extending the length to increase sensitivity due to attenuation.

The TPPS molecules inside the SCF are freely stacked on the wall of the holes and the aggregate change is considered more significant than the sensor we have previously reported using the same dye in [29]. In that case, TPPS is encapsulated and partially bonded to the matrix film on the tip of a multi-mode optical fibre, which may have led to the higher sensitivity of the SCF (the theoretical detection limit is 0.02 ppm as compared to 0.15 ppm reported in [29]). However, the reversibility in ambient conditions of the SCF sensor is not as good as the sensor reported in [29], it shows a slow recovery rate after removal from ammonia atmosphere to ambient and it did not fully recover under 12 hours observation. However, HCl vapours help the sensor to recover quickly which leads to a reusable sensor that requires refreshment with HCl.

The sensor response to ammonia is due to the deprotonation of the porphyrin ring of the TPPS by an ammonia molecule. Other amines such as putrescine or cadaverine which are malodours and often released in the putrefying tissue of dead bodies [40] will confound the sensor measurement due to the same amine group. This sensor could also be useful for monitoring seafood quality and safety in relation to biogenic amines [41]. Acidic gas such as H_2S, HF, HCl will also affect the sensor response due to the protonation process to the dye molecules, but high concentration of such gases are unlikely to be present in air.

The SCF sensor demonstrates detection of ammonia odor as low as 150 ppb (0.15 ppm) which is far lower than human can sense nasally (> 5 ppm) and far lower than the recommended safety levels (25 ppm). Therefore it can be useful for indoor ammonia safety monitoring in places such as the fertiliser manufacturing industry, livestock feeding industry and coal mines where electrical spark can be dangerous due to explosive gases. The ratiometric method ensures the signal is independent of the temperature fluctuation. The temperature-dependent intensity change of a single wavelength also reveals the potential of temperature measurement simultaneous with ammonia measurement.

A comparison of the ammonia sensors mentioned in the introduction is listed in the table.1 along with remarks on the Pros and Cons of each sensor. Notably, the SCF sensor reported here has demonstrated the lowest detected NH_3 among all the optical fibre sensors. In addition, the reported colourimetric sensor also has great advantages over the fluorescent-based measurement in terms of applications due to the all-fibre sensing structure and direct interaction of dye to ammonia. The latter is the only previously reported dye functionalised microstructured optical fibre for ammonia sensing comparable to our research.

Sensitivity can be improved further by optimising the thickness of the sensing film. A thicker film generally provides higher sensitivities due to extended chemical interaction under the effective region of the evanescent field which varies depending on the coating refractive index and operation wavelength. Once the film becomes thicker than the evanescent field region, further increase in sensitivity does not occur. Improvement in the coating process would allow better control of film thickness to optimise sensitivity. Film deposition inside of such a fibre is the biggest challenge when adapting it for chemical sensing due to the small diameter of the holes. In this work, a simple approach of filling up and drying out is applied which allows coating at ambient pressure. However, this method is not ideal as the film may not deposit uniformly across the fibre (as indicated by the simulation model). The uniformity

can be improved in future with pretreatment of the fibre with plasma to increase the surface hydrophilicity of the inner wall of the fibre [42]. Layer-by-layer nanoassembly via electrostatic force between two oppositely charged molecules can be adapted for this dye to generate a uniform coating [43]. This method involves multiple exposures of different liquids and washing steps so that a pressurised flow system is required to exchange liquid inside of the fibre holes [17].

V. CONCLUSION

An ammonia gas sensor constructed with dye functionalised microstructure optical fibre is demonstrated. The ammonia-sensitive dyes are deposited in the inner wall of the holes of an SCF which, in line with other optical fibres between light source and detector, form an all fibre ammonia sensing structure. A numerical simulation of the optical transmission properties of the proposed dye-functionalised SCF sensor is conducted. The simulation results demonstrate that ~0.02% of the total optical power exist in the air holes of the SCF which interacts with absorbing dye deposited on the walls leading to a selective loss in transmission intensity which matches the trend observed in the experiment. The sensor demonstrates high sensitivity and reusable features for ammonia gas detection with a minimum detectable concentration of 0.15 ppm demonstrated experimentally and a theoretical limit of detection of 0.02 ppm. No significant temperature cross-sensitivity is observed with a ratiometric measurement of intensities at two different wavelengths. The response time ($T_{10-90\%}$) and recovery time ($T_{90-10\%}$) are 160 s and 225 s, respectively.

Table.1 A summary of ammonia sensors in the introduction

Sensing platform	Method	Sensor size	Lowest detected NH_3	Remark
4-NH3-100, commercial NH3 sensor from Honeywell (Reference sensor)	Electrochemical	Ø:2 cm H: 1.6 cm (sensor head)	0.15 ppm	**Pros:** relatively cheap for the overall system; Good sensitivity for atmosphere monitoring. **Cons:** Relatively large size compared to optical fibre based sensor; cannot be applied in a hazardous environment.
Hollow optical waveguide [27]	Gas absorption spectroscopy	Length: 3 m	7-14 ppm	**Pros:** Multi-gas detection **Cons:** Bulky size
Suspended-core-fibre functionalised with SnO_2/ITO nanofilm [28]	Fabry-Perot interferometer	Ø: ~120 µm Length: ~700 µm	10 ppm	**Pros:** sensing region is small; Reflection probe is easy to use. **Cons:** Susceptible to RH due to water molecule adsorption on metal oxide.
Microstructured polymer optical fibre functionalised with eosin [33]	Fluorescent measurement	Ø: 780 µm Length: N/A	50 ppm	**Pros:** Use of matrix film for dye encapsulation, easy for co-doping other chemicals. **Cons:** Require operation in humidified atmosphere; Open space measurement with lens, susceptible to ambient light.
Standard multimode optical fibre probe coated with TPPS in a sol-gel matrix film [29]	Colorimetric measurement	Ø: ~120 µm Film thickness < 10 µm On the fibre tip	0.3 ppm	**Pros:** Small size**;** Reflection probe, easy to apply. **Cons:** The sensing film is exposed which could be contaminated in some applications.
Suspended-core-fibre functionalised with TPPS (This work)	Colorimetric measurement	Ø: ~120 µm Length: 7 cm	0.15 ppm (theoretical detection limit:20 ppb)	**Pros:** High sensitivity; Intrinsic design with protection from contamination. **Cons:** Size is relatively larger than the tip-based structure.

REFERENCES

[1] C. Elosua, *et al*., "Optical fiber sensing applications: detection and identification of gases and volatile organic compounds," *Fiber Optic Sensors. Intech,* pp. 27-52, 2012.

[2] L. Alwis, *et al*., "Developments in optical fibre sensors for industrial applications," *Optics & Laser Technology,* vol. 78, pp. 62-66, 2016.

[3] R. Correia, *et al*., "Biomedical application of optical fibre sensors," *Journal of Optics,* vol. 20, no. 7, Art.no. 073003, 2018.

[4] L. Liu, *et al*., "A reflection-mode fibre-optic sensor for breath carbon dioxide measurement in healthcare," *Sensing and Bio-Sensing Research,* vol. 22, Art.no.100254, 2019.

[5] A. Kaushik, et al, "Nanostructured gas sensors for health care: an overview," *Journal of personalized nanomedicine,* vol. 1, no. 1, p. 10, 2015.

[6] T. Liu *et al.*, "Fibre optic sensors for coal mine hazard detection," *Measurement,* vol. 124, pp. 211-223, 2018.

[7] F. Formenti and A. D. Farmery, "Intravascular oxygen sensors with novel applications for bedside respiratory monitoring," *Anaesthesia,* vol. 72, no. S1, pp. 95-104, 2017.

[8] K. P. Hansen, "Introduction to nonlinear photonic crystal fibers," *Journal of Optical and Fiber Communications Reports,* vol. 2, no. 3, pp. 226-254, 2005.

[9] H. Ademgil and S. Haxha, "Endlessly single mode photonic crystal fiber with improved effective mode area," *Optics Communications,* vol. 285, no. 6, pp. 1514-1518, 2012.

[10] A. Ortigosa-Blanch *et al.*, "Highly birefringent photonic crystal fibers," *Optics Letters,* vol. 25, no. 18, pp. 1325-1327, 2000.

[11] Z. Tang *et al.*, "A U-shape fibre-optic pH sensor based on hydrogen bonding of ethyl cellulose with a sol-gel matrix," *Journal of Lightwave Technology,*vol.38, no. 5, pp. 1557-1564, 2021.

[12] S. Korposh, *et al*., "Tapered optical fibre sensors: Current trends and future perspectives," *Sensors,* vol. 19, no. 10, Art.no. 2294, 2019.

[13] A. Webb, *et al*., "Suspended-core holey fiber for evanescent-field sensing," *Optical Engineering,* vol. 46, no. 1, Art.no. 010503, 2007.

[14] J. M. Fini, "Microstructure fibres for optical sensing in gases and liquids," *Measurement Science and Technology,* vol. 15, no. 6, p. 1120, 2004.

[15] W. Jin, *et al*., "Gas detection with micro- and nano-engineered optical fibers," *Optical Fiber Technology,* vol. 19, no. 6, Part B, pp. 741-759, 2013.

[16] D. Lopez-Torres, *et al*., "Optical Fiber Sensors Based on Microstructured Optical Fibers to Detect Gases and Volatile Organic Compounds—A Review," *Sensors,* vol. 20, no. 9, Art.no. 2555, 2020.

[17] B. Doherty *et al.*, "Nanoparticle functionalised small-core suspended-core fibre–a novel platform for efficient sensing," *Biomedical optics express,* vol. 8, no. 2, pp. 790-799, 2017.

[18] L. Wang *et al.*, "Mid-Infrared Gas Detection Using a Chalcogenide Suspended-Core Fiber," *Journal of Lightwave Technology,* vol. 37, no. 20, pp. 5193-5198, 2019.

[19] P. Jaworski *et al.*, "Antiresonant hollow-core fiber-based dual gas sensor for detection of methane and carbon dioxide in the near-and mid-infrared regions," *Sensors,* vol. 20, no. 14, Art.no. 3813, 2020.

[20] M. Morshed, M. I. Hassan, T. K. Roy, M. S. Uddin, and S. A. Razzak, "Microstructure core photonic crystal fiber for gas sensing applications," *Applied optics,* vol. 54, no. 29, pp. 8637-8643, 2015.

[21] S. H. Kassani, et al., "Fast response in-line gas sensor using C-type fiber and Ge-doped ring defect photonic crystal fiber," *Optics Express,* vol. 21, no. 12, pp. 14074-14083, 2013.

[22] C. M. Wathes, et al., "Ammonia concentrations and emissions in livestock production facilities: guidelines and limits in the USA and UK," in *2003 ASAE Annual Meeting*, 2003.

[23] N. Roney and F. Llados, "Toxicological profile for ammonia," 2004.

[24] G. Dooly, et al., "Highly selective optical fibre ammonia sensor for use in agriculture," *Procedia Engineering,* vol. 25, pp. 1113-1116, 2011.

[25] R. Claps, et al., "Ammonia detection by use of near-infrared diode-laser-based overtone spectroscopy," *Applied Optics,* vol. 40, no. 24, pp. 4387-4394, 2001.

[26] R. Woodward, et al., "Swept-wavelength mid-infrared fiber laser for real-time ammonia gas sensing," *APL photonics,* vol. 4, no. 2, Art.no. 020801, 2019.

[27] G. J. Fetzer, et al., "Tunable diode laser absorption spectroscopy in coiled hollow optical waveguides," *Applied Optics,* vol. 41, no. 18, pp. 3613-3621, 2002.

[28] D. López-Torres *et al.*, "Sensitivity optimization of a microstructured optical fiber ammonia gas sensor by means of tuning the thickness of a metal oxide nano-coating," *IEEE Sensors Journal,* vol. 19, no. 13, pp. 4982-4991, 2019.

[29] L. Liu, *et al*., "Multi-Parameter Optical Fiber Sensing of Gaseous Ammonia and Carbon Dioxide," *Journal of Lightwave Technology,* vol. 38, no. 7, pp. 2037-2045, 2020.

[30] M. Maierhofer, *et al*., "Optical ammonia sensors based on fluorescent aza-BODIPY dyes— a flexible toolbox," *Analytical and Bioanalytical Chemistry,* vol. 412, no. 27, pp. 7559-7567, 2020.

[31] A. J. Rodríguez, et al., "A fiber optic ammonia sensor using a universal pH indicator," *Sensors,* vol. 14, no. 3, pp. 4060-4073, 2014.

[32] J.F. Li, *et al*., "Plasmon-enhanced fluorescence spectroscopy," *Chemical Society Reviews,* vol. 46, no. 13, pp. 3962-3979, 2017.

[33] L. Peng *et al.*, "Gaseous ammonia fluorescence probe based on cellulose acetate modified microstructured optical fiber," *Optics Communications,* vol. 284, no. 19, pp. 4810-4814, 2011.

[34] T. M. Monro *et al.*, "Sensing with suspended-core optical fibers," *Optical Fiber Technology,* vol. 16, no. 6, pp. 343-356, 2010.

[35] L. Bolzonello, et al., "Delocalized triplet state in porphyrin J-aggregates revealed by EPR spectroscopy," *Physical Chemistry Chemical Physics,* vol. 19, no. 40, pp. 27173-27177, 2017.

[36] M. A. Castriciano, *et al*., "Structural rearrangements in 5, 10, 15, 20-tetrakis (4-sulfonatophenyl) porphyrin J-aggregates under strongly acidic conditions," *The journal of physical chemistry B,* vol. 107, no. 34, pp. 8765-8771, 2003.

[37] K. Gut and M. Pamuła, "Investigating the Attenuation Changes of Modes Guided in Waveguides with Absorbing Cover," *Molecular and Quantum Acoustics,* vol. 22, pp. 187-196, 2001.

[38] R. A. Kadhim, et al., "Highly Sensitive D-Shaped Optical Fiber Surface Plasmon Resonance Refractive Index Sensor Based on Ag-α-Fe2O3 Grating," *IEEE Sensors Journal,* vol. 20, no. 17, pp. 9816-9824, 2020.

[39] M. E. Webber *et al.*, "Agricultural ammonia sensor using diode lasers and photoacoustic spectroscopy," *Measurement Science and Technology,* vol. 16, no. 8, Art.no. 1547, 2005.

[40] A. Hussain *et al.*, "High-affinity olfactory receptor for the death-associated odor cadaverine," *Proceedings of the National Academy of Sciences,* vol. 110, no. 48, pp. 19579-19584, 2013.

[41] K. Biji, *et al*., "Biogenic amines in seafood: a review," *Journal of food science and technology,* vol. 53, no. 5, pp. 2210-2218, 2016.

[42] L. Zou, *et al*., "Surface hydrophilic modification of RO membranes by plasma polymerization for low organic fouling," *Journal of Membrane Science,* vol. 369, no. 1-2, pp. 420-428, 2011.

[43] S. Korposh, *et al*., "Porphyrin-nanoassembled fiber-optic gas sensor fabrication: Optimization of parameters for sensitive ammonia gas detection," *Optics & Laser Technology,* vol. 101, pp. 1-10, 2018.